Pflügers Arch (1994) 427:406–413

Pflügers Archiv
European Journal of Physiology

Point mutations in IIS4 alter activation and inactivation of rat brain IIA Na channels in *Xenopus* oocyte macropatches

Andrea Fleig[1]*, James M. Fitch[3], Alan L. Goldin[4], Martin D. Rayner[1], John G. Starkus[2], Peter C. Ruben[2]

[1] Department of Physiology, John A. Burns School of Medicine, University of Hawaii, Honolulu, HI 96822, USA
[2] Békésy Laboratory of Neurobiology, University of Hawaii, Honolulu, HI 96822, USA
[3] Department of Physiology and Biophysics, University of California, Irvine, CA 92717, USA
[4] Department of Microbiology and Molecular Genetics, University of California, Irvine, CA 92717, USA

Received September 6, 1993/Received after revision January 11, 1994/Accepted January 14, 1994

Abstract. Macroscopic currents of wild-type rat brain IIA (RBIIA) and mutant Na channels were recorded in excised patches from *Xenopus* oocytes. A charge deletion (K859Q) and an adjacent conservative mutation (L860F) in the second domain S4 membrane-spanning region differentially altered voltage sensitivity and kinetics. Analysis of voltage dependence was confined to Na currents with fast inactivation kinetics, although RBIIA and K859Q (but not L860F) also showed proportional shifts between at least two gating modes, rendering currents with fast or slow inactivation kinetics, respectively. Compared to RBIIA, the midpoint of the activation curve was shifted in both K859Q and L860F by 22 mV to more positive potentials, yet this shift was not associated with a corresponding change in the voltage dependence of time constants for activation (τ_a) or inactivation (τ_{h1}, τ_{h2}). L860F showed faster activation time constants τ_a than RBIIA, while K859Q was slower for both the activation (τ_a) and the inactivation components (τ_{h1}). Similarly, the steady-state inactivation curve of L860F but not K859Q shifted by 9 mV in the hyperpolarizing direction. Thus, the fourth charge in the IIS4 transmembrane segment exerts control over voltage sensitivity and kinetics of activation and may interact with structure that influence other aspects of channel gating.

Key words: Sodium channel – Oocyte – Patch clamp

Introduction

Na channels are principally responsible for the rising phase of electrogenic action potentials in nerve and muscle. The tetrameric structure of the membrane-spanning protein has been deduced [4, 10, 14] and properties of activation and inactivation gating [20, 22, 23] and selectivity [8] have been attributed to various regions of the protein. The fourth membrane-spanning segment in each domain contains a high proportion of positively charged residues with, typically, a lysine or arginine in every third position. The S4 segment in the first domain (IS4) has been shown to be associated with activation gating by site-directed mutagenesis [20]; charge deletion or reversal altered the voltage sensitivity of channel activation as measured by changes in the slope and midpoint of conductance versus voltage [$g(V)$] curves. On the other hand, that study [20] reported little effect on channel gating by single charge deletions of IIS4, whereas double mutations that included both IIS4 charge deletions and IIS4 deletions paired with IS4 deletions did shift the voltage sensitivity of channel activation to a greater extent than the IS4 deletion alone. By contrast, a neutral mutation (L860F) in the IIS4 segment at a position adjacent to the fourth charge affected the voltage sensitivity of channel gating by producing a +20 mV shift in the peak of the current versus voltage [$I(V)$] curve without a detectable change in valence [5].

We have attempted to resolve these findings by directly comparing cell-free macroscopic recordings of a single mutation involving the fourth charge in the IIS4 segment with a mutation of the adjacent leucine residue. Thus, we have compared the voltage sensitivity as well as the kinetics of wild-type rat brain IIA (RBIIA) Na channels with a mutation of the fourth charge in IIS4 (K859Q) and an apparently conservative mutation of the adjacent position (L860F). Here we report that these mutations similarly alter activation voltage sensitivity while differentially affecting kinetics of Na channel activation as well as the voltage sensitivity of steady-state inactivation. Our findings suggest a multiplicity of effects that include direct as well as indirect involvement of the IIS4 segment with channel gating.

Materials and methods

Construction of Na channel mutations. The pVA2580 plasmid contains the wild-type rat IIA Na channel α subunit following a T7

* *Present address:* Max-Planck-Institute for Biophysical Chemistry, Department of Membrane Biophysics, Am Fassberg, D-37077 Göttingen, Germany
Correspondence to: A. Fleig

RNA polymerase promoter [5]. The pVA200 plasmid contains the L860F mutation, which is the Na channel α subunit cDNA clone orginally isolated by Auld et al. [4] following an SP6 promoter. The pVA2580 *XmaI*/*Sph*I fragment containing the wild-type Na channel domain II S4 segment was subcloned into an m13 phage with a custom polylinker. Uracil-containing single-stranded DNA was synthesized by growth in the *dut-, ung- E. coli* strain RZ1032 [11]. To mutate the lysine at position 859 in domain II S4, a kinased oligonucleotide primer (GGACTTTGCCAACT/ CGGAAGACTCTAAG) was annealed to the template at a 10:1 molar ratio. The primer was extended with T4 DNA polymerase (2.5 units) in the presence of T4 DNA ligase (6 Weiss units) in a 100 µl reaction containing 100 mM tris(hydroxymethyl)aminomethane (Tris)HCl (pH 7.5), 50 mM $MgCl_2$, 2.5 mM 2′-deoxyadenosine 5′-triphosphate (dATP), 2.5 mM 2-deoxycytidine 5′-triphosphate (dCTP), 2.5 mM 2-deoxyguanosine 5′-triphosphate (dGTP) 2.5 mM thymidine 5′-triphosphate (TTP), 2.5 mM adenosine 5′-triphosphate (ATP), and 1 mM dithiothreitol (DTT). The reaction was incubated on ice for 5 min, at 22−26° C for 5 min, then at 37° C for 2 h. Reaction products were ethanol precipitated and resuspended in 20 µl H_2O. *E. coli* strain XL-1 (*ung*+) was electroporated using 1 µl of the synthesis reaction, and plaques were picked and used to generate single-stranded DNA which was then screened by dideoxynucleotide sequencing to confirm the mutation of lysine to glutamine. The *Xma*I to *Sph*I fragment containing the mutation was then ligated into the full-length cDNA clone pVA2580, which was confirmed by sequencing.

Expression of mRNA in Xenopus oocytes. Na channel cDNA from RBIIA and the mutants K859Q and L860F served as a template for standard in vitro transcription to yield mRNA. Oocytes for mRNA injection were obtained from laboratory-reared female *Xenopus laevis* (Nasco Biologicals) and enzymatically isolated by bathing them for 1−2 h in Ca^{2+}-free oocyte-Ringer (OR-2) containing (in mM): NaCl 82.5, KCl 2, $MgCl_2$ 1, 4-(2-hydroxyethyl)-1-piperazineethanesulfonic acid (HEPES) 5, pH 7.5, with 2 mg/ml collagenase (Boehringer-Mannheim) added. An automatic nanoinjector (Drummond Scientific) was used to inject individual oocytes with mRNA.

Electrophysiological measurements. Expression testing of oocytes was performed with the two-electrode voltage clamp (TEV, Dagan) after 4−7 days of incubation at 16° C. Na channel expression proved sufficient for macropatch recording between days 4 and 7 after microinjection of mRNA. Oocytes which had at least a 2-µA whole-cell current were chosen for patch-clamp recording following removal of their vitelline membrane after exposure to a hyperosmotic solution containing (in mM): K-glutamate 200, KCl 20, $MgCl_2$ 1, ethylenebis(oxonitrilo)tetraacetate (EGTA) 10, HEPES 10, pH 7.4. Patch electrodes (aluminosilicate, Sutter Instruments) were pulled in five stages, fire-polished and coated with Sylgard. The pipette solution (ND96) contained (in mM): NaCl 96, KCl 4, $CaCl_2$ 1.8, $MgCl_2$ 1, HEPES 5, pH 7.4. The bath solution (ISOP) contained (in mM): NaCl 9.6, KCl 88, $CaCl_2$ 1, $MgCl_2$ 1, EGTA 11, HEPES 5, pH 7.4.

Experimental methods and analysis. All experiments were performed at room temperature (20−24° C). Data aquisition and analysis was made with an EPC-9 patch-clamp amplifier controlled by an ITC-16 interface (Instrutech) and a Macintosh Quadra 750 computer running Pulse and PulseFit software (HEKA). IGOR software (WaveMetrics) was used for kinetic analysis and graphing.

Data shown are from three to seven oocytes out of at least two separate injection batches. Each oocyte yielded two to five patches that could be analyzed. All data records were acquired by averaging four sweeps and low-pass filtered at a cutoff frequency of 11.3 kHz. The number n refers to patches unless indicated otherwise. Student's t-test or paired t-test was used for statistical evaluation. $I(V)$ relationships were approximated by the product of a linear term and a Boltzmann function according to the equation:

$$g_{max} \cdot (V_m - E_{Na}) \cdot [1/1 + \exp^{-z(V_m - V_{1/2})/kT}]$$

where g_{max} is the maximal conductance, V_m the test potential, E_{Na} the reversal potential, z the valence, $V_{1/2}$ the voltage at half-maximal activation, k the Boltzmann constant, and T the absolute temperature. Steady-state activation and inactivation data were fitted by a Boltzmann function according to the equation:

$$1/1 + \exp^{-z(V_m - V_{1/2})kT}.$$

The sum of three exponential functions describing the rising phase and the biphasic current decline were fitted to current traces to determine time constants (τ) and the intercepts of the functions at t = O for activation (A_a) and inactivation (A_{h1}, A_{h2}) according to the function:

$$(A_a \cdot \exp^{-t/\tau_a}) + (A_{h1} \cdot \exp^{-t/\tau_{h1}}) + (A_{h2} \cdot \exp^{-t/\tau_{h2}}) + A_{offset}$$

where t is time, and A_{offset} the baseline. Depending on the relative amplitude A_{h2} and peak current (I_{max}), we refer to Na currents with amplitude ratios A_{h2}/I_{max} of < 0.4 as showing fast kinetic behavior.

Results

Na currents in excised macropatches

Figure 1 depicts typical examples of Na currents recorded from inside-out macropatches excised from *Xenopus* oocytes expressing the α subunit of RBIIA (A), K859Q (B) and L860F (C). Current families of RBIIA and K859Q evoked by depolarizing voltage steps could have either fast (traces in left column) or rather slow inactivation kinetics (traces in right column). The proportion of patches exhibiting slow Na currents was 70% for RBIIA and 27% for K859Q. L860F displayed only fast inactivation kinetics in this study. The overall appearance of inactivation kinetics in current traces is based on the equilibrium between at least two distinguishable gating modes [12], as observed previously in macroscopic currents from excised macropatches from *Xenopus* oocytes [6]. Only currents which could be categorized as showing fast kinetic behavior (see Materials and methods) were considered for further analysis here, so as to segregate voltage shifts induced by changes in gating mode from those induced by the mutations.

Mutations in IIS4 affect voltage sensitivity

Figure 2 illustrates the $I(V)$ relationship (Fig. 2A) and the voltage dependence of activation (Fig. 2B) from Na currents of RBIIA (●) and mutants K859Q (■) and L860F (□). A 200-ms prepulse to −150 mV preceded each test pulse and proved sufficient to remove any residual steady-state inactivation occurring at the holding potential (−100 mV). Channel activation and peak amplitude of both K859Q and L860F is shifted to more positive potentials by 20 mV as compared to RBIIA (Fig. 2A, $P \ll 0.001$, Student's t-test), whereas reversal potentials do not change (RBIIA: $+45 \pm 3.3$ mV, K859Q: $+48 \pm 1.8$ mV and L860F: $+47.6 \pm 1.2$; means $\pm$ SD, n = 5, 14 and 14, respectively). Figure 2B shows the steady-state activation characteristics of

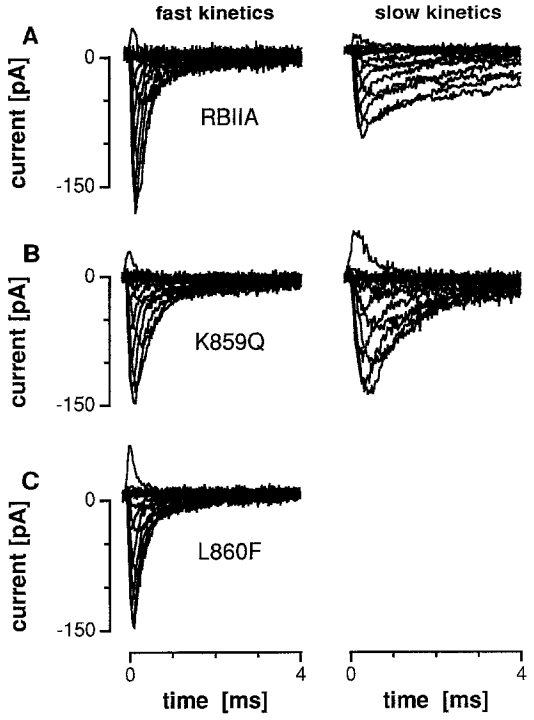

Fig. 1 A–C. Macroscopic Na currents in oocyte excised macropatches. Current families recorded in excised macropatches from oocytes injected with unitary mRNA as encoded by RBIIA, K859Q and L860F. Inactivation kinetics of RBIIA (**A**) and K859Q (**B**) could predominated by fast or slow kinetics (*left* and *right columns* respectively) whereas L860F (**C**) displayed only fast kinetics in this study. The mean amplitude ratios A_{h2}/I_{max} for the analyzed patches showing fast inactivation kinetics were 0.18 ± 0.1 for RBIIA and 0.25 ± 0.1 for K859Q (see Materials and methods; $n = 5$ and 14, respectively). Holding potential was -100 mV. A conditioning prepulse to -150 mV for 200 ms preceded a 10-ms test pulse to remove slow inactivation. Test potentials ranged between -60 mV to $+60$ mV (**A, B**) and -80 mV to $+60$ mV (**C**). Test pulse frequency was 0.5 Hz. A P/4 procedure was applied to substract linear leak and capacitive transient currents from the raw data

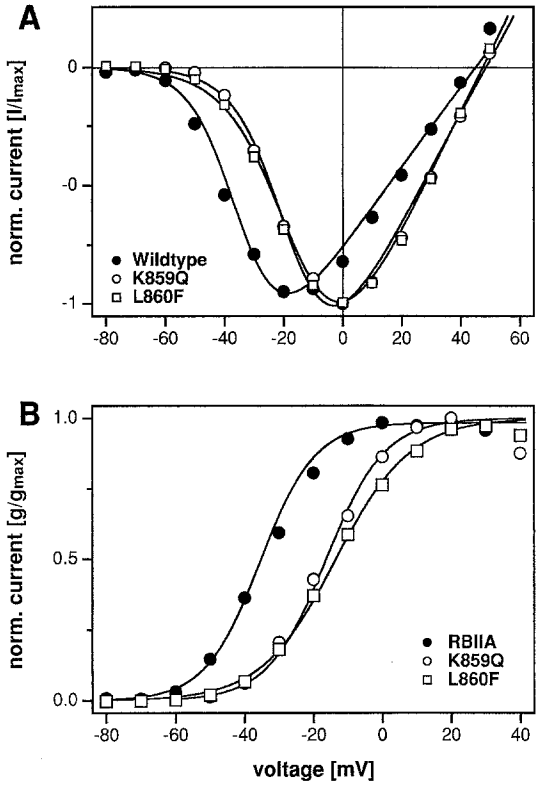

Fig. 2 A, B. Voltage dependence of activation and fraction of open channels. **A** Normalized mean peak current amplitudes (I/I_{max}) are plotted against test potential (mV) with corresponding mean current vs. voltage [$I(V)$] fits of RBIIA (●), K859Q (○) and L860F (□) ($n = 5$, 14 and 14, respectively). The channels activate half-maximally at $V_{1/2(RBIIA)} = -33.8 \pm 3.3$ mV, $V_{1/2(K859Q)} = -14.2 \pm 9$ mV and $V_{1/2(L860F)} = -14.3 \pm 3.1$ mV (means ± SD, respectively). **B** The peak currents have been normalized for maximal conductance (g_{max}), expressed as a fraction of open channels for RBIIA (●), K859Q (○) and L860F (□) and plotted as a function of variable test pulses preceded by a constant conditioning prepulse of -150 mV (duration: 200 ms) (see Materials and methods). Half-maximal open probabilities of channels are $V_{1/2(RBIIA)} = -35.4 \pm 7$ mV, $V_{1/2(K859Q)} = -13.3 \pm 11$ mV and $V_{1/2(L860F)} = -13.4 \pm 3$ mV (n = as in Fig. 2A). Valences, z, are $z_{RBIIA} = 3.2 \pm 0.27$, $z_{K859Q} = 2.9 \pm 0.26$ and $z_{L860F} = 2.3 \pm 0.2$. Data were acquired at room temperature (20–24 °C)

RBIIA and mutant Na currents. The peak currents have been normalized for maximal conductance and expressed as a fraction of open channels $F(V)$. The midpoint $V_{1/2}$ of the $F(V)$ curve is indicative of the probability that 50% of channels will open at the test potential. The slope of the $F(V)$ curve suggests the effective valence of channel activation. When compared to RBIIA Na currents, half-maximal activation of both K859Q and L860F is shifted to the right along the voltage axis by 20 mV (same n as in Fig. 2A, $P \ll 0.001$). Only L860F resulted in a statistically significant reduction in the slope valence as compared to RBIIA ($z_{RBIIA} = 3.2 \pm 0.27$, $z_{K859Q} = 2.9 \pm 0.3$ and $z_{L860F} = 2.3 \pm 0.2$; mean ± SD $P \ll 0.001$ for L860F). Comparing the mutants with each other shows that the valence for activation differs at a probability level of $P \ll 0.001$.

Fast inactivation and slow inactivation have been shown to be two independent processes, which can be pharmacologically separated [7, 15, 17], and are differentially selected for depending on the prepulse length [16]. To assess fast inactivation (h_∞) on channel availability, short prepulses of few milliseconds duration (2–10 ms) precede the test pulse. To reach equilibrium of slow inactivation (s_∞), the prepulses have to be substantially longer (> 50 ms). Increasing prepulse durations from a few milliseconds to several hundred milliseconds can shift the midpoint of the inactivation curve to more negative potentials (e.g. [18]).

We looked at fast inactivation (h_∞) and steady-state inactivation (s_∞) from Na currents of RBIIA and mutants K859Q and L860F using pulse protocols with variable prepulse potentials of 5 ms and 200 ms in length, respectively. In all cases, the prepulse was preceded by a 200-ms conditioning pulse to -150 mV and followed by a 10-ms test pulse to 0 mV. For RBIIA Na channels expressed in *Xenopus* oocytes, longer prepulse lengths than 200 ms did not affect midpoint values of the s_∞ curve. Figure 3 illustrates the s_∞ curves for all three

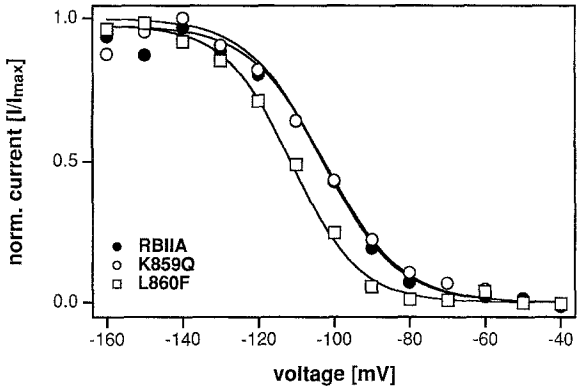

Fig. 3. Steady-state inactivation curves of RBIIA, K859Q and L860F. Data show the normalized mean peak amplitudes of RBIIA (●), K859Q (○) and L860F (□), as indicated in the graph. s_∞ data were determined from a constant test pulse to 0 mV and plotted as a function of variable conditioning prepulses (duration: 200 ms). Half-maximal availabilities, as determined by Boltzmann fits to individual data sets, are $V_{1/2(RBIIA)} = -102 \pm 5$ mV, $V_{1/2(K859Q)} = -103 \pm 9.2$ mV and $V_{1/2(L860F)} = -111 \pm 9$ mV (means ± SD, n = 5, 8 and 12, respectively). Valences are $z_{RBIIA} = 2.5 \pm 0.9$, $z_{K859Q} = 2.5 \pm 0.43$ and $z_{L860F} = 2.8 \pm 0.47$. These parameters were used to compute the superimposed fits in the graph. Data were acquired at room temperature (20–24° C)

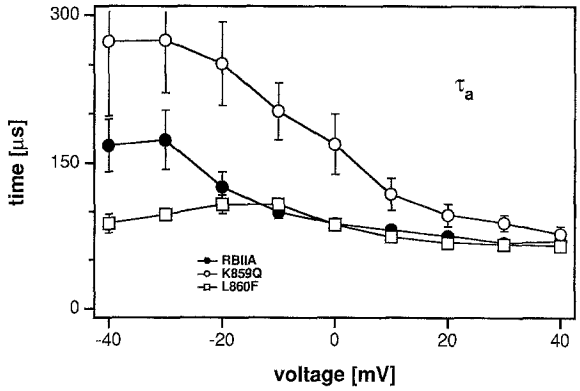

Fig. 4. Voltage dependence of the activation time constants τ_a. Time constants τ_a for activation of RBIIA (●), K859Q (○) and L860F (□) plotted as function of test potential. Each point represents values of mean time constants ± SEM (10 current families each). Recordings were made at room temperature (20–24° C)

channel species. Half-maximal availability of RBIIA (●) and K859Q (○) channels coincide in midpoint values, whereas L860F (□) is shifted by 9 mV to more negative potentials as compared to RBIIA ($P < 0.003$, n = 5, 8 and 12, respectively). Valences of the s_∞ curves are not affected. Not illustrated are fast inactivation data (h_∞) for RBIIA, K859Q and L860F, where the midpoint voltages of RBIIA and L860F are not statistically different, but K859Q is shifted to the right by 7 mV ($P < 0.02$, $V_{1/2\ RBIIA} = -78 \pm 9$ mV, $V_{1/2\ K859Q} = -71 \pm 4$ mV and $V_{1/2\ L860F} = -82 \pm 5$ mV, n = 4, 5 and 10, respectively). The valences for both mutations are reduced ($P < 0.02$, $z_{RBIIA} = 3 \pm 0.5$, $z_{K859Q} = 2 \pm 0.2$ and $z_{L860F} = 2 \pm 0.27$). These results are summarized in Table 1.

Mutant differentially affect τ_a

Kinetic analysis of current traces from RBIIA and mutant channels was performed to assess whether the shifts in voltage sensitivity were associated with corresponding shifts in channel kinetics. Concurrent tri-exponential analysis of individual traces rendered time constants for the rising phase τ_a and the two decaying phases τ_{h1} and τ_{h2} (see Materials and methods).

Figure 4 shows τ_a values of RBIIA (●), K859Q (○) and L860F (□) as a function of test potential (n = 5, 8 and 10, respectively) recorded at room temperature (20–24° C). K859Q activates more slowly than RBIIA, whereas L860F is faster at more negative potentials ($P < 0.006$ and $P < 0.03$, respectively; assessed by Student's paired t-test). At this point it cannot be evaluated if L860F activates faster than RBIIA at higher potentials, as the cutoff frequency used in this study limits the resolution of very fast time constant values. Comparing τ_a values of K859Q and L860F across voltage reveals that they differ significantly ($P < 0.03$). Evaluating time con-

Table 1. Parameters of RBIIA, K859Q and L860F

Parameters		Na channel type		
		wild-type RBIIA	K859Q	L860F
Activation	$V_{1/2}$	− 35 ± 7 mV	− 16 ± 7 mV****	− 13 ± 3 mV****
	z	3.2 ± 0.27	2.9 ± 0.3	2.3 ± 0.2****
s_∞	$V_{1/2}$	−102 ± 5 mV	−103 ± 9 mV	−111 ± 5 mV***
	z	2.5 ± 0.36	2.5 ± 0.4	2.8 ± 0.47
h_∞	$V_{1/2}$	− 78 ± 9 mV	− 71 ± 4 mV**	− 82 ± 5 mV
	z	3.0 ± 0.5	2.3 ± 0.2**	2.0 ± 0.27
Time constant at −10 mV	τ_a	100 ± 20 µs	203 ± 66 µs**	107 ± 16 µs
	τ_{h1}	168 ± 48 µs	270 ± 50 µs*	170 ± 30 µs
	τ_{h2}	2.2 ± 0.8 ms	3.2 ± 1.8 ms	2 ± 0.7 ms

$V_{1/2}$, Half-maximal voltage; z, valence; s_∞, steady-state inactivation; h_∞, fast inactivation. The table lists the parameters (± SD) evaluated for RBIIA, K859Q and L860F.
**** $P < 0.001$; *** $P < 0.003$; ** $P < 0.02$; * $P < 0.04$ for data as compared to the wild-type RBIIA data

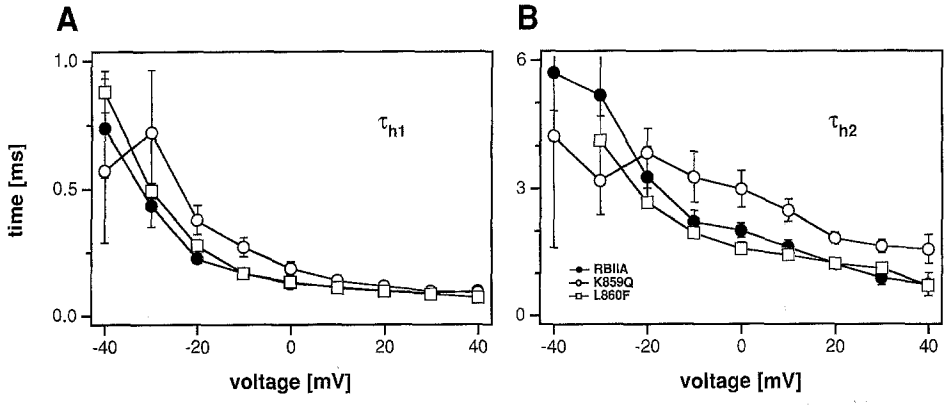

Fig. 5A,B. Voltage dependence of inactivation time constants τ_{h1} and τ_{h2}. Time constants τ_{h1} and τ_{h2} for the two inactivation components of RBIIA (●), K859Q (○) and L860F (□) are plotted as function of test potential. Each *point* represents values of mean time constants ± SEM (10 current families each). Recordings were made at room temperature (20–24° C)

stants at −10 mV, only τ_a values of K859Q showed significant differences as compared to RBIIA ($P < 0.02$) with $\tau_{a(RBIIA)} = 100 \pm 20$ µs, $\tau_{a(K859Q)} = 203 \pm 66$ µs and $\tau_{a(860F)} = 107 \pm 16$ µs (means ± SD, $n = 5$, 8 and 10, respectively).

Voltage dependence of τ_{h1} and τ_{h2} for RBIIA (●), K859Q (○) and L860F (□) is shown in Fig. 5A and B, respectively. τ_{h1} values of K859Q are slower than RBIIA with $P < 0.05$ ($n = 5$, 8 and 10, respectively), whereas the τ_{h1} value of L860F is not altered. Likewise, looking at the test potential of −10 mV, K859Q, but not L860F, shows significant differences of the time constant τ_{h1} as compared to RBIIA ($P < 0.04$, $\tau_{h1(RBIIA)} = 168 \pm 48$ µs, $\tau_{h1(K859Q)} = 270 \pm 50$ µs and $\tau_{h1(L860F)} = 170 \pm 30$ µs; means ± SD, $n = 5$, 8 and 10, respectively). Comparing the voltage dependence of τ_{h1} values of K859Q with L860F shows that L860F inactivates faster than K859Q ($P < 0.03$). No statistically significant differences could be detected for the voltage dependence of τ_{h2} comparing RBIIA and mutants, or mutants with each other (Fig. 5B; $n = 5$, 8 and 10, respectively). Equally, time constants at −10 mV are $\tau_{h2(RBIIA)} = 2.2 \pm 0.8$ ms, $\tau_{h2(K859Q)} = 3.2 \pm 1.8$ ms and $\tau_{h2(L860F)} = 2 \pm 0.7$ ms with no observed statistical difference (means ± SD, same n as for τ_{h1}).

Overall, the right shifts in the $F(V)$ curves of K859Q and L860F are not matched by equivalent shifts in the voltage dependence of time constants (Table 1). Although the slower activation of K859Q might be explained by a similar effect for both $F(V)$ and τ_a in that mutant, no such shift is apparent in the L860F kinetics.

Discussion

We have seen that: (1) neutralization of the fourth charge in IIS4 at position 859 changes the $F(V)$ curve midpoint by +20 mV and decreases the rates of both activation and the τ_{h1} component of fast inactivation; (2) replacement of a leucine with an apparently neutral phenylalanine at the 860 position shifts the $F(V)$ curve by +20 mV, decreases effective valence of activation, changes the s_∞ curve by −10 mV, and increases the rate of activation, without affecting inactivation rates. Thus, despite the similar effects on the $F(V)$ curve of charge neutralization and an adjacent conservative mutation, these mutations have opposite effects on the rates of activation, and differing effects on activation valence, steady-state inactivation and fast inactivation component τ_{h1}.

A charge neutralization and an apparently conservative mutation similarly affect activation voltage sensitivity

Both K859Q and L860F mutations shift the activation curve some 20 mV in the depolarizing direction. In addition, L860F decreases the effective valence of activation by as much as 0.9e in comparison to wild-type RBIIA, whereas K859Q did not cause a significant change in valence. The right-shift imposed on the activation voltage sensitivity by L860F has been previously noted by Auld et al. [5]. However, the resolution of their data, obtained with TEV clamp, did not distinguish the decrease in activation valence. Using cell-attached macropatches, Stühmer et al. [20] noted similar shifts in the midpoint of the activation curve with the K859Q/K862Q double mutation and with the K226Q/K859Q/K862Q triple mutation. The triple mutation gave the greatest effect whereas K862Q alone did not produce a voltage shift in the activation curve. Although the results presented by Stühmer et al. [20] did not include a study of K859Q alone, their data in combination with the present study indicate that IIS4 and, more specifically, K859 (but not K862) are important determinants of activation voltage sensitivity.

Our results are similar to those of Tytgat et al. [21] who reported that, in RCK1 channels, neutralization of the fifth positive charge in the S4 putative membrane-spanning region caused a positive shift in the activation curve. The fifth charge in K channels is homologous to the 859 position in IIS4 of the Na channel. Tytgat et al. [21] did not observe a change in activation valence with the RCK1 K5I mutation and therefore concluded that the fifth charge is not an activation voltage sensor. If homology in function as well as structure is assumed to exist between K channels and Na channels, then by extension it is possible that the lysine at position 859 in RBIIA should not directly participate in activation gating.

Similarly, it is not yet clear whether the IIS4 components studied here directly control activation gating by

functioning as a voltage sensor, or indirectly exert control over gating through interactions with other components of the channel protein. The marginal effect produced by neutralization of the 859 charge might indicate a voltage sensing role if confirmed in a larger experimental series. However, the coincident effects of the L860F mutation suggests other possible interpretations. Of these, interactions with other gating control components seems the most parsimonious explanation.

Effects of mutations on steady-state and fast inactivation voltage sensitivity

Fast and low inactivation may be readily distinguished by their characteristically different pharmacological sensitivities. The enzymatic agents that selectively remove fast inactivation [7, 15, 17] can alter the voltage sensitivity of slow inactivation; yet in the presence of these agents, slow inactivation remains intact. Thus, it should be re-emphasized that fast and slow inactivation are separate processes [1, 13, 16] mediated by pharmacologically distinct mechanisms [17]. However, the steady-state inactivation measured by s_∞ curve protocols is, presumably, a mixture of fast and slow inactivation, whose relative contributions are dependent on prepulse duration. For purely practical reasons, we have here used a prepulse durations of 5 ms to study fast inactivation and 200 ms to approximate the true steady-state of these inactivation processes. Although 200 ms is the maximum time that we dared expose excised macropatches to extreme prepulse voltages, 200 ms may not be long enough to reach a fully equilibrated distribution (as represented by the $F(V_h)$ curve; see [16]).

The L860F mutation moves the 200-ms s_∞ curve by -10 mV relative to RBIIA. This is particularly remarkable given the observation that the L860F mutation shifts the activation curve by $+20$ mV. We have previously hypothesized that slow inactivation is a parallel process coupled to activation [16, 19]. The present results support this interpretation so far as slow inactivation contributes to the s_∞ curve. If slow inactivation was a direct consequence of channel activation (like fast inactivation, see [2, 3]), then we would expect that both activation and steady-state inactivation curves should be shifted in the same direction and should be affected to about the same extent by mutations that influence either one or the other process. By contrast, the results presented here independently support the concepts of parallel voltage sensitivity for steady-state inactivation and some form of coupling between activation and steady-state inactivation, since L860F differentially affects both activation and steady-state inactivation parameters. The s_∞ curve for K859Q approximately superimposes with that of RBIIA. By the same argument, this observation suggests that the K859Q mutation may also alter the coupling between activation and steady-state inactivation (with a -80 mV change in midpoint from the $F(V)$ curve to the s_∞ curve, as compared to a -60 mV midpoint shift for RBIIA), but to a lesser extent than L860F (with a -90 mV change in midpoint).

Since neither of the mutations studied here appreciably alters the valence of steady-state inactivation, it seems unlikely that IIS4 could be the voltage sensor for steady-state inactivation. Thus, our results suggest that interactions between the voltage sensor for activation and that for steady-state inactivation might be linked through IIS4, and that this link has been altered by the L860F mutation and to a lesser extent by K859Q.

The h_∞ curves (following a 5-ms prepulse) for RBIIA and L860F approximately superimpose with midpoints at about -80 mV. This may be coincidental, however, since inactivation midpoints are dependent upon prepulse duration [16]. Whereas the midpoint of voltage sensitivity for RBIIA shifts between the $F(V)$ extreme of approximately -35 mV and the steady-state extreme of approximately -102 mV, the L860F midpoints shift between approximately -13 mV and -111 mV (see Table 1 and below). Therefore, the midpoints of the RBIIA and L860F curves must necessarily coincide at some prepulse duration. Thus, our preliminary data (not shown) indicates that the h_∞ curve for L860F lies to the right of that for RBIIA with prepulse durations shorter than 5 ms, and to the left with prepulse durations longer than 5 ms. By contrast, the midpoint of the h_∞ curve for K859Q is at about -70 mV. Although significantly different from the RBIIA and L860F h_∞ midpoints, the $+10$ mV shift is not unexpected. As discussed above, K859Q voltage sensitivity undergoes a -80 mV shift from the $F(V)$ position to the steady-state, compared to the -90 mV shift for L860F.

Implications of kinetic changes imposed by mutations

We have previously reported a time-dependent transition from a predominantly slow inactivation mode to a predominantly fast inactivation mode in wild-type Na channels [6, 9, 12, 24]. Here we extend those observations to the present study only in so far as to note that K859Q shows similar time-dependent changes in the relative contribution of fast and slow inactivation rates as RBIIA. In contrast, L860F channels have thus far only been observed to have primarily fast inactivation kinetics. However, it is important to note that inactivation of L860F channels does indeed show two well-separated kinetic components the rates of which are comparable to those seen in wild-type channels. Thus, both τ_{h1} and τ_{h2} are readily apparent in L860F, the vast majority of L860F channels inactivate via the fast pathway. We have not observed any time-dependent transitions in the activation gating mode of L860F channels.

Only fast mode channels have been compared for the purposes of the present study. Although the sample rate used to collect data did not allow very high resolution of activation rates, the difference between τ_a for K859Q and τ_a for RBIIA and L860F is substantial over a wide range of test potentials. One interpretation of the relatively slow kinetics of K859Q channels is that IIS4 participates directly in channel gating and that the neutralization of a charge results in a less responsive voltage sensor, both in terms of time and voltage dependence.

By contrast, L860F channels activate slightly faster than RBIIA. We only observe these differences over a limited range of test potentials, but our resolution of activation kinetics was limited by sample rate. A higher sample rates and/or slower kinetics (e.g. at low temperatures) we might find that L860F is faster than RBIIA and K859Q over a wider range of test potentials.

This difference between the activation kinetic effects of K859Q as opposed to L860F could suggest that the two mutations might influence activation gating in different ways: K859Q through direct alteration of IIS4 voltage sensitivity and L860F through indirect interactions with other gating segments (e.g. IS4). The relatively small increase in activation rate by L860F, and the limited test potential range over which its affect was visible does not provide a particularly strong case for this argument. However, additional data at higher sample rates should clarify this hypothesis.

All the channel types studied here show two well-separated and distinguishable rates of inactivation. The apparent slowing of both τ_{h1} and τ_{h2} in K859Q relative to RBIIA and L860F can be largely accounted for by the corresponding decrease in its activation rate. Thus, both τ_{h1} and τ_{h2} seem to represent different forms of fast inactivation whose voltage dependence and kinetics may be expected to follow that of activation.

Conclusions

How can an apparently neutral mutation shift the $F(V)$ curve 20 mV in the depolarizing direction, the s_∞ curve in the hyperpolarizing direction, and increase the rates of activation and fast inactivation? How can another mutation similarly shift the $F(V)$ curve 20 mV in the depolarizing direction, yet not affect the s_∞ curve and actually decrease activation and inactivation rates? The dual and disparate effects of L860F and K859Q on the voltage sensitivities of activation and inactivation suggest that IIS4 might be both a voltage sensor for activation and be linked to the voltage sensitive components that control slow inactivation. This is a profound set of effects and could explain previous observations that L860F expression is typically lower than RBIIA [5], since those studies assessed L860F from a holding potential of -100 mV, at which well over half the channels would be slow inactivated and thus unavailable for opening.

The range of effects we see on kinetics and voltage sensitivity points to independent control of the parameters at the structural level. In a system of first order reactions, the midpoint is determined by relative well-depth, valence is determined by particle charge, and reaction rate is determined by barrier height. Our present findings suggest that these reaction parameters may be manipulated in complex ways via mutations of a single residue. It seems unlikely that different S4 segments are voltage sensors for single, identifiable, physiological parameters. Rather the S4 segments represent a complexly coupled system of voltage sensitive elements (see also [5, 16, 21]). Thus we speculate that physiologically identifiable parameters derive from the interactive properties of many structural components in the Na channel protein.

Acknowledgements. This study was supported in part by National Institutes of Health (NIH) Grant no. RO1 NS29204 (P. C. Ruben), no. RO1 NS21151 (J. G. Starkus), grants-in-aid from the American Heart Association (Hawaii Affiliate) (J. G. Starkus, P. C. Ruben), NIH training grant NS-07351 (J. M. Fitch), NSF Grant no. IBN-9221984, and the Lucille P. Markey Foundation (A. L. Goldin).

References

1. Adelman WJ, Palti Y (1969) The effects of external potassium and long duration voltage conditioning on the amplitude of sodium currents in the giant axon of the squid, *Loligo peali*. J Gen Physiol 54:589–606
2. Aldrich RW, Corey CP, Stevens CF (1983) A reinterpretation of mammalian sodium channel gating based on single channel recording. Nature 306:436–441
3. Armstrong CM, Bezanilla F (1977) Inactivation of the sodium channel. II. Gating current experiments. J Gen Physiol 70:567–590
4. Auld VJ, Goldin AL, Krafte DS, Marshall J, Dunn JM, Catterall WA, Lester HA, Davidson N, Dunn RJ (1988) A rat brain Na^+ channel α subunit with novel gating properties. Neuron 1:449–461
5. Auld VJ, Goldin AL, Krafte DS, Catterall WA, Lester HA, Davidson N (1990) A neutral amino acid change in segment IIS4 dramatically alters the gating properties of the voltage-dependent sodium channel. Proc Natl Acad Sci USA 87:323–327
6. Fleig A, Ruben PC, Rayner MD (1994) Kinetic mode switch of rat brain IIA sodium channels in *Xenopus* oocytes excised macro patches. Pflügers Arch 427:399–405
7. Heggeness ST, Starkus JG (1986) Saxitoxin and tetrotoxin. Electrostatic effects on sodium channel gating in crayfish giant axons. Biophys J 49:629–643
8. Heinemann S, Terlau H, Stühmer W, Imoto K, Numa S (1992) Calcium channel characteristics conferred on the sodium channel by single mutations. Nature 356:441–443
9. Joho RH, Moorman JR, VanDongen AMJ, Kirsch GE, Silberberg H, Schuster G, Brown AM (1990) Toxin and kinetic profile of rat brain type III sodium channels expressed in *Xenopus* oocytes. Mol Brain Res 7:105–113
10. Kayano T, Noda M, Flockerzi V, Takahashi H, Numa S (1988) Primary structure of rat brain sodium channel III deduced from the cDNA sequence. FEBS Lett 228:187–194
11. Kunkel TA (1985) Rapid and efficient mutagenesis without phenotypic selection. Proc Natl Acad Sci USA 82:488–492
12. Moorman JR, Kirsch GE, VanDongen AMJ, Joho RH, Brown AM (1990) Fast and slow gating of sodium channels encoded by a single mRNA. Neuron 4:243–252
13. Narahashi T (1974) Chemicals as tools in the study of excitable membrane. Physiol Rev 54:813–889
14. Noda M, Shimizu S, Tanabe T, Takai T, Kayano T, Ikeda T, Takahashi H, Nakayama H, Kanaoka Y, Minamino N, Kangawa K, Matsuo H, Raftery M, Hirose S, Inayama H, Hayashida T, Miyata T, Numa S (1984) Primary structure of *Electrophorus electricus* sodium channel deduced from cDNA sequence. Nature 312:121–127
15. Quandt FN (1987) Burst kinetics of sodium channels which lack fast inactivation in mouse neuroblastoma cells. J Gen Physiol 392:563–585
16. Ruben PC, Starkus JG, Rayner MD (1992) Steady state availability of sodium channels: interactions between slow inactivation and activation. Biophys J 61:941–955
17. Rudy B (1978) Slow inactivation of the sodium conductance in squid giant axons. Pronase resistance. J Physiol (Lond) 283:1–21

18. Ruff R, Simoncini L, Stühmer W (1987) Comparison between slow sodium channel inactivation in rat slow- and fast-twitch muscle. J Physiol (Lond) 383:339–348
19. Starkus JG, Rayner MD, Fleig A, Ruben PC (1993) Photodynamic modification of sodium channels by methylene blue: effects on fast and slow inactivation. Biophys J 65:715–726
20. Stühmer W, Conti F, Suzuki H, Wang X, Noda M, Yahagi N, Kubo H, Numa S (1989) Structural parts involved in activation and inactivation of the sodium channel. Nature 339:597–603
21. Tytgat J, Nakazawa K, Hess P (1993) Cooperative and non-cooperative subunit interactions determine voltage-dependent K^+ channel gating. Biophys J 64:A226
22. Vassilev PM, Scheuer T, Catterall WA (1989) Identification of an intracellular peptide segment in sodium channel inactivation. Science 241:1658–1661
23. West JW, Scheuer T, Maechler L, Catterall WA (1992) Efficient expression of rat brain type IIA Na^+ channel α subunits in a somatic cell line. Neuron 8:59–70
24. Zhou J, Potts JF, Trimmer JS, Agnew WS, Sigworth FJ (1991) Multiple gating modes and the effect of modulating factors on the μI sodium channel. Neuron 7:775–785